



Reconstruction of the reconnection rate from magnetic field disturbances in an incompressible plasma

V. S. Semenov¹, T. Penz^{2,3}, M. F. Heyn⁴, I. B. Ivanov⁵, I. V. Kubyshkin¹,
H. K. Biernat^{3,2,6}, and V. V. Ivanova¹

¹Institute of Physics, State University, St. Petersburg, 198504 Russia

²Institute for Theoretical Physics, Universitätsplatz 5, A-8010 Graz, Austria

³Space Research Institute, Austrian Academy of Sciences,
Schmiedlstraße 6, A-8042 Graz, Austria

⁴Institut für Theoretische Physik, Technische Universität Graz,
Petersgasse 16, A-8010 Graz, Austria

⁵Petersburg Nuclear Physics Institute, Gatchina, 188300 Russia

⁶Institute for Geophysics, Astrophysics, and Meteorology,
University of Graz, Universitätsplatz 5, A-8010 Graz, Austria

ABSTRACT

We present a theoretical model to describe the behaviour of flux transfer events. Based on a time-dependent Petschek-type model of reconnection we are able to evaluate the magnetic field configuration and the flow components, as well as the shape of the Petschek shocks. We consider two different kinds of hypothetical measurements, namely along a profile $B_z(x)$ and along a trajectory $B_z(t)$. Our aim is to solve an inverse problem to achieve the reconnection rate from the magnetic field data. By using a discrete Fourier transformation, we are able to calculate the magnetic field along a certain profile $B_z(x)$. Out of this profile, we reconstruct the reconnection electric field at the reconnection site. This is an ill-posed inverse problem, which we treat with the method of regularisation. With this method, we can reconstruct the reconnection electric field out of profiles. But realistic satellite measurements are always trajectories and we use the so-called Cagniard-deHoop method to calculate the magnetic field configuration along a trajectory $B_z(t)$. The solution is given as a convolution integral, which is a well-known problem in the theory of inverse problems. By using a regularisation operator, we can reconstruct the reconnection electric field for different initial electric field configurations. It is shown that this method works well for distances up to 50 times the height of the outflow region.

2 INTRODUCTION

In a search for reconnection at the dayside magnetopause, Russell and Elphic (1978) ([1]) noticed that there appear localized, transient reconnection events. These events last only about a minute and have a magnetic field signature, which suggests that there is some kind of bubble or tube-like disturbance moving along the magnetopause. Russell and Elphic interpreted these events as isolated tubes of magnetic flux, connecting magnetosheath field lines with magnetospheric field lines, and called them flux transfer events, or FTEs for short [2]. A FTE is identified by an isolated bipolar variation of the magnetic field component normal to the magnetopause with an amplitude well above the ambient level of fluctuations and a simultaneous deflection in the tangential components, associated with generally enhanced field strength (for a discussion of the L–M–N coordinate system, which is used here, see [1]). The occurrence of FTEs is strongly correlated with the direction of the North–South component of the interplanetary magnetic field (IMF) with virtually no FTEs present, when the field is purely northwards [3, 4]. The implications of time-varying, localized reconnection models for the interpretation of FTEs have been discussed by, e.g., [5]. The suggestion that FTEs are a manifestation of time-varying reconnection at the magnetopause has been verified by numerical, time-dependent MHD simulations [6].

After the observation of these FTE signatures, some attempts were made to reconstruct different features of the reconnection process involved. Southwood (1985) ([7]) predicted that FTE signatures would be observed by a satellite regardless of whether or not it actually penetrates the FTE. Farrugia et al. (1987) ([8]) verified Southwood’s suggestion and showed that FTE-like signatures could be generated without the satellite is penetrating the obstacle. Walthour et al. (1993, 1994) ([9, 10]) developed a method for inferring the cross-sectional size, shape, and the speed of propagation of a thin, infinitely long obstacle. Since the analysis is confined to perturbations outside the obstacle, the method is referred to as a remote sensing method. Lawrence (1998) ([11]) applied this method to a series of FTE-like events generated by a time-dependent model of reconnection, where he studied the effects of three different reconnection fields on the perturbations. Also the robustness of the remote sensing method was tested [12]. Additionally, Sonnerup and co-worker [13, 14, 15] developed a method to reconstruct two-dimensional space plasma structures in magnetohydrostatic equilibrium. Hu and Sonnerup (2003) ([15]) applied this model to two magnetopause crossings by the spacecraft AMPTE/IRM, and reconstructed field structures. But these models do not intend to reconstruct the reconnection electric field.

In this paper we present different methods to reconstruct the reconnection electric field E^* for the first time. The main approach is to solve an ill-posed inverse problem by using a regularisation method developed by Tikhonov and Arsenin [16]. We introduce a method based on a discrete Fourier transformation which enables us to reconstruct the reconnection electric field from a profile $B_z(x)$. For this case, we use a regularisation parameter for the reconstruction, but a profile is not realistic for measurements of a satellite. Therefore, we use the Cagniard–deHoop method [17, 18, 19, 20], which allows to calculate the disturbances in the ambient magnetic field along trajectories $B_z(t)$. Using this method, the solution for the magnetic field is given as a convolution integral $B_z = K * E^*$, which is well-known in the theory of ill-posed inverse problems. In Laplace space, the convolution integral is given as $B_z(p) = K(p) E^*(p)$, and we use a regularisation operator to reconstruct the reconnection electric field for different initial cases.

This paper is organized as follows: In the next two sections, the time-dependent Petschek-type model for asymmetric reconnection and its mathematical formulation are presented. In Section 4, a model for determining the magnetic field configuration from a profile based on a Fourier transformation are discussed, followed by a short

introduction to inverse problems and regularisation theory applied to a profile (Section 5). Thereafter, we give a short description of the Cagniard–deHoop method to calculate the magnetic field along a trajectory. In Section 7 we apply the inverse theory to reconstruct different initial electric fields from a trajectory.

3 THE PETSCHKEK–TYPE MODEL FOR MAGNETIC RECONNECTION

We consider a geometry of oppositely directed magnetic fields, which are separated by an infinitely thin tangential discontinuity. Across a tangential discontinuity, the normal components of the magnetic field and plasma velocity are zero ($B_n = 0$, $v_n = 0$). To fulfill the Rankine–Hugoniot relations, the density and the tangential components of the magnetic field and velocity may change arbitrarily, subject only to the requirement that the total pressure, which is the sum of the thermal and the magnetic pressure, $p + B^2/(8\pi)$, stays constant [21]. Since there is no mass flow and no magnetic connection across a tangential discontinuity, there will be no electric field component along it ($E_t = 0$). Now we assume that the plasma conductivity is decreased in a certain region, the so-called diffusion region. Some mechanisms proposed for this process are: *a*) the onset of some instability leading to the excitation of turbulent waves and causing the local decrease of the conductivity [22, 23], *b*) stochastic dynamics of high-energy charged particles [24], and *c*) collisionless reconnection with electron inertia, where the Hall term is included and brings in the dynamics of whistler waves (see, e.g., the GEM magnetic reconnection program, [25, 26]). Corresponding to the decrease of conductivity is the appearance of a reconnection electric field, and therefore a normal component of the magnetic field will be produced [27]. A tangential discontinuity is a marginal stable situation, because in the system free energy is stored in the form of tangential stresses due to the shear of the plasma flow and the magnetic field. Any local deviation of the perfect conductivity approximation due to the reconnection electric field will cause a reconfiguration of the system. Therefore, the magnetic field can diffuse and the resulting magnetic flux through the surface sets free stored energy from the unbalanced tangential stresses. The surface gets non-linearly unstable and decays into a system of MHD wave modes. The most general scheme of a decay looks like $S^+(R^+)AS^-(R^-)C(T)S^-(R^-)AS^+(R^+)$ [28], where S^+ , S^- are fast and slow shocks, R^+ , R^- are fast and slow rarefaction waves, and A, C, T are Alfvén, contact and tangential discontinuities, respectively.

One can see, that the calculation of the plasma and magnetic field parameters in each zone between the discontinuities is extremely difficult in its complete realisation [29]. To simplify the problem, we introduce the restriction of so-called weak reconnection [30] which implies, that the reconnection electric field E^* is much smaller than the Alfvén electric field $E_A = v_A B_0/c$, where B_0 and $v_A = B_0/\sqrt{4\pi\rho}$ are the initial magnetic field and the Alfvén velocity, respectively. Thus, we can introduce a small parameter

$$\epsilon = \frac{E^*}{E_A} \ll 1. \quad (1)$$

Within this restriction, we are considering small components of the magnetic field and velocity in a direction normal to the tangential discontinuity:

$$B_n^2 \ll B_t^2, \quad (2)$$

$$\rho v_n^2 \ll p + \frac{B_t^2}{8\pi}. \quad (3)$$

Thus, to lowest order, the total pressure is conserved across the discontinuity. As a result, there is no pressure gradient that could drive a strong fast shock. Further, in the incompressible case $\rho = const$, which is considered in the following, the Alfvén wave merges with

the slow shock, whereby the downstream tangential magnetic field is switched-off, forming a so-called Petschek shock. These Petschek shocks bound a region of accelerated and heated plasma, the field reversal or outflow region [31]. The pairs of shocks are moving in opposite direction away from the site, where reconnection was initiated. In this outflow region, the magnetic fields from opposite sides are connected (Figure 1). After some time, the reconnection electric field has dropped to zero and the outflow regions become detached from the diffusion region and continue to propagate along the tangential discontinuity.

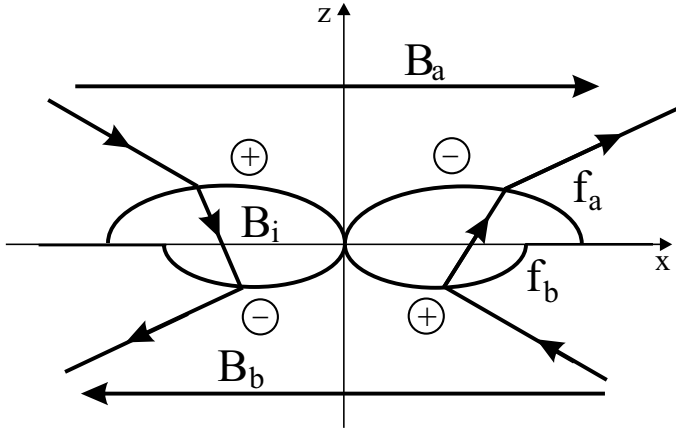


Figure 1: Magnetic field configuration for asymmetric reconnection. B_a and B_b denote the magnetic field strength in the upper and the lower half plane, respectively. B_i is the magnetic field strength in the outflow region, and the thick lines indicate the shape of the Petschek shocks f_a and f_b . The plus and minus symbols indicate the signs in Equation (18). The current sheet separating the two inflow regions is located in the x - y plane, where y completes the right hand coordinate system.

4 MHD DESCRIPTION OF ASYMMETRIC RECONNECTION

4.1 Basic equations

In this section, we perform a MHD analysis of the case of asymmetric reconnection. The basic configuration is shown in Figure 1. The magnetic fields are orientated antiparallel and have different field strength, namely B_a in the upper half plane, and B_b in the lower half plane. The background magnetic fields and the total pressure P are assumed to be constant. Additionally, we consider a fixed plasma, meaning that $\mathbf{v} = 0$ in the inflow region in zero order. The reconnection line is directed along the y -axis, where y completes the right hand coordinate system, and the diffusion region is located at $x = 0$. The shocks f_a and f_b bound the outflow region, where the magnetic field is B_i . The current sheet separating the two different plasmas is located in the x - y plane.

We consider the incompressible case, where $\rho = \text{const}$, and introduce normalized quantities, since they are convenient for the computational analysis of the problem. The normalization is done with respect to the initial magnetic field B_0 , the initial Alfvén velocity v_A , the time duration of a reconnection pulse T_0 , the Alfvén electric field E_A , and the length scale $v_A T_0$. Now it is possible to write the MHD equations for an ideal, incompressible fluid in normalized form as [32]

$$\frac{\partial \mathbf{v}}{\partial t} + (\mathbf{v} \cdot \nabla) \mathbf{v} = -\nabla P + (\mathbf{B} \cdot \nabla) \mathbf{B}, \quad (4)$$

$$\frac{\partial \mathbf{B}}{\partial t} = \nabla \times (\mathbf{v} \times \mathbf{B}), \quad (5)$$

$$\nabla \cdot \mathbf{v} = 0, \quad (6)$$

$$\nabla \cdot \mathbf{B} = 0, \quad (7)$$

where \mathbf{B} , \mathbf{v} , and P are the magnetic field, the plasma flow velocity, and the total pressure, respectively. In addition to continuous solutions, this set of equations also allows for solutions including discontinuities. In the incompressible case, where the energy equation is not needed, the Rankine–Hugoniot relations across the discontinuity must be satisfied [33]

$$\llbracket B_n \rrbracket = 0, \quad (8)$$

$$\llbracket m \rrbracket = 0, \quad (9)$$

$$\llbracket P \rrbracket = 0, \quad (10)$$

$$\llbracket B_n v_t - m B_t \rrbracket = 0, \quad (11)$$

$$\llbracket m v_t - B_n B_t \rrbracket = 0, \quad (12)$$

where subscripts n and t denote directions normal and tangential to the shock surface. If we perform an order-of-magnitude estimation, we can use the assumption for weak reconnection that quantities perpendicular to the current sheet are small

$$P_i, v_{ix}, B_{ix}, x \propto 1, \quad (13)$$

and

$$v_{iz}, B_{iz}, z f \propto \epsilon, \quad (14)$$

where $f(x, t)$ denotes the shape of the shocks. Now the problem can be separated in two different steps. First we can evaluate the tangential components B_{ix} and v_{ix} from the non-linear system of MHD equations for the zero order by assuming that B_{ix} and v_{ix} are constant. If they are constant, they can be found from the Rankine–Hugoniot relations directly. In a second step, we can determine the components B_{iz} and v_{iz} from the linearized system of MHD equations in the first order approximation.

To perform the first step, the unit normal vector \mathbf{n} is introduced by using the moving surface $\varphi(x, z, t) = z - f(x, t) = 0$ to get $\mathbf{n} = \nabla \varphi / |\nabla \varphi|$. It follows that

$$\mathbf{n} = (-f_x, 1), \quad (15)$$

with $f_x = \frac{\partial f}{\partial x}$. The corresponding shock speed is

$$u_n = f_t. \quad (16)$$

Now we can find the tangential components from solving the non-linear set of equations in zeroth order. It is convenient to introduce a parameter $\lambda = B_n/m$, which is continuous across the shock. Using this parameter, Equations (11) and (12) can be written as

$$\lambda \llbracket v_t \rrbracket = \llbracket B_t \rrbracket = 0,$$

and

$$\lambda \llbracket B_t \rrbracket = \llbracket v_t \rrbracket = 0,$$

respectively. Since $\lambda^2 = 1$, $\lambda = \pm 1$ and the shock relations (11, 12) can be simplified to

$$v_n - u_n = \pm B_n, \quad (17)$$

and

$$\llbracket v_t \rrbracket = \pm \llbracket B_t \rrbracket. \quad (18)$$

The sign in these two equations is defined by the initial configuration. If the direction of the magnetic field is the same as the direction of the flow velocity, which is always directed from the inflow to the

outflow region, we have to take the plus sign, otherwise the minus sign (Figure 1). Now we can calculate the magnetic field and the velocity in the outflow region by solving the Riemann problem for this case. Using Equation (18) gives

$$v_{ix} - 0 = -(B_{ix} - B_a),$$

for the upper half-plane. Since $\mathbf{v} = 0$ outside the outflow region and used the minus sign, since the direction of B_n and v_n are opposite. For the lower half-plane we have to take the plus sign, since B_n and v_n have the same direction and we achieve

$$v_{ix} - 0 = B_{ix} - B_b.$$

Now we have two equations for two unknowns and we can evaluate the x -components of the magnetic field and the velocity in the outflow region as

$$B_{ix} = \frac{B_a + B_b}{2}, \quad (19)$$

and

$$v_{ix} = \frac{B_a - B_b}{2}. \quad (20)$$

One can see if we suppose that B_{ix} and v_{ix} are constant, they fulfill the differential set of MHD equations as well as the shock relations. Therefore, we found the solution for the non-linear problem.

4.2 The displacement vector

The second step is to evaluate the normal components from the linearized set of MHD equations by introducing the displacement vector. We can write the normalized induction equation (5) as

$$\frac{\partial \mathbf{B}}{\partial t} = (\mathbf{B} \cdot \nabla) \mathbf{v} - (\mathbf{v} \cdot \nabla) \mathbf{B}. \quad (21)$$

After linearisation we get

$$\frac{\partial \mathbf{B}^{(1)}}{\partial t} + (\mathbf{v}_0 \cdot \nabla) \mathbf{B}^{(1)} = (\mathbf{B}_0 \cdot \nabla) \mathbf{v}^{(1)} \quad (22)$$

where (1) denotes first-order quantities. Now we can introduce the displacement vector ξ in the following way:

$$\mathbf{B}^{(1)} = (\mathbf{B}_0 \cdot \nabla) \xi, \quad (23)$$

$$\mathbf{v}^{(1)} = \frac{d\xi}{dz} = \frac{\partial \xi}{\partial t} + (\mathbf{v}_0 \cdot \nabla) \xi. \quad (24)$$

It is obvious that by using this two definitions, Equation (22) is automatically satisfied, if \mathbf{B}_0 and \mathbf{v}_0 are constant. It can also be seen from Equation (23) that $\nabla \cdot \xi = 0$. If we consider the linearized equation of motion

$$\frac{\partial \mathbf{v}^{(1)}}{\partial t} + (\mathbf{v}_0 \cdot \nabla) \mathbf{v}^{(1)} = -\nabla P^{(1)} + (\mathbf{B}_0 \cdot \nabla) \mathbf{B}^{(1)}, \quad (25)$$

and substitute the displacement vector, we get

$$\begin{aligned} \frac{\partial^2 \xi}{\partial t^2} + (\mathbf{v}_0 \cdot \nabla) \frac{\partial \xi}{\partial t} + (\mathbf{v}_0 \cdot \nabla) \frac{\partial \xi}{\partial t} + (\mathbf{v}_0 \cdot \nabla)^2 \xi = \\ = \frac{d^2}{dt^2} \xi = -\nabla P^{(1)} + (\mathbf{B}_0 \cdot \nabla)^2 \xi. \end{aligned} \quad (26)$$

Now we have to consider the pressure balance across the outflow region. If we use the order-of-magnitude estimations (13, 14) for the normalized equation of motion (4), we achieve

$$\frac{\partial v_{iz}}{\partial t} + v_{ix} \frac{\partial v_{iz}}{\partial x} + v_{iz} \frac{\partial v_{iz}}{\partial z} = -\frac{\partial P_i}{\partial z} + B_{ix} \frac{\partial B_{iz}}{\partial x} + B_{iz} \frac{\partial B_{iz}}{\partial z}.$$

In this equation all terms are of order $\mathcal{O}(\epsilon)$ except the pressure gradient, which is of order $\mathcal{O}(1/\epsilon)$. This means that the value of this term is much larger than the values of the other terms, and so it must be zero

$$\frac{\partial P_i^{(0)}}{\partial z} = \frac{\partial P_i^{(1)}}{\partial z} \equiv 0, \quad (27)$$

because otherwise all other terms are negligible. Thus, the pressure is only a function of x

$$P_i^{(1)} = P_i^{(1)}(x), \quad (28)$$

and

$$P_i^{(0)} = \text{const}. \quad (29)$$

From Equation (26), we achieve the following equations in the upper and lower half plane for the z -components as

$$\frac{d^2}{dt^2} \xi_{az} - \left(B_a \frac{\partial}{\partial x} \right)^2 \xi_{az} = -\frac{\partial P_a^{(1)}}{\partial z}, \quad (30)$$

and

$$\frac{d^2}{dt^2} \xi_{bz} - \left(B_b \frac{\partial}{\partial x} \right)^2 \xi_{bz} = -\frac{\partial P_b^{(1)}}{\partial z}. \quad (31)$$

Now we have to match both equations. Since $\nabla \cdot \xi = 0$, Equation (26) gives

$$\Delta P_{a,b}^{(1)} = 0, \quad (32)$$

in both half planes. The boundary condition at $z = 0$ is given as $P_a^{(1)}(x, z = 0, t) = P_b^{(1)}(x, z = 0, t)$. Therefore, $P_a^{(1)}(x, z, t) = P_b^{(1)}(x, -z, t)$ across the discontinuity. This can be written as

$$\frac{\partial P_a^{(1)}}{\partial z} \Big|_{z=0} = -\frac{\partial P_b^{(1)}}{\partial z} \Big|_{z=0}, \quad (33)$$

leading to the matching of both equations as

$$\frac{d^2}{dt^2} \xi_{az} - B_a^2 \frac{\partial^2}{\partial x^2} \xi_{az} + \frac{d^2}{dt^2} \xi_{bz} - B_b^2 \frac{\partial^2}{\partial x^2} \xi_{bz} = 0. \quad (34)$$

This is the basic equation, which will enable us to calculate all quantities we need to describe the case of asymmetric reconnection.

Our aim is now to evaluate the z -component of the displacement vectors in the inflow regions ξ_{az} and ξ_{bz} . The components of the magnetic field in the inflow regions are

$$\mathbf{B}_a = \left(B_a + B_a \frac{\partial}{\partial x} \xi_{ax}, B_a \frac{\partial}{\partial x} \xi_{az} \right), \quad (35)$$

and

$$\mathbf{B}_b = \left(B_b + B_b \frac{\partial}{\partial x} \xi_{bx}, B_b \frac{\partial}{\partial x} \xi_{bz} \right), \quad (36)$$

whereas the magnetic field in the outflow region is

$$\mathbf{B}_i = \left(B_{ix}, B_{ix} \frac{\partial}{\partial x} \xi_{iz} \right). \quad (37)$$

Evaluating Equation (8) across the shock in the upper half plane, we get

$$-B_a \frac{\partial}{\partial x} f_a + B_a \frac{\partial}{\partial x} \xi_{az} = -B_{ix} \frac{\partial}{\partial x} f_a + B_{ix} \frac{\partial}{\partial x} \xi_{iz},$$

where f_a denote the shape of the shock in the upper half plane. After integration with respect to x we achieve

$$-B_a f_a + B_a \xi_{az} = -B_{ix} f_a + B_{ix} \xi_{iz}.$$

Now we can write the z -component of the displacement vector in the inflow region a as

$$\xi_{az} = \frac{B_{ix} \xi_{iz} + v_{ix} f_a}{B_a}, \quad (38)$$

where we used equations (19) and (20) to get $B_a - B_{ix} = v_{ix}$. The same can be done for the shock f_b to get in the same way the z -component of the displacement vector in the inflow region b as

$$\xi_{bz} = \frac{B_{ix} \xi_{iz} - v_{ix} f_b}{B_b}. \quad (39)$$

Here we used the fact that $B_b - B_{ix} = -v_{ix}$. Now we know the displacement vectors, but we still do not know the shape of the shocks.

4.3 The shape of the shocks

To get the shape of the shocks f_a and f_b we must also consider the velocities in the different regions. Using Equation (24), we get the velocities in first order in the inflow regions as

$$\mathbf{v}_a = \left(\frac{\partial}{\partial t} \xi_{ax}, \frac{\partial}{\partial t} \xi_{az} \right), \quad (40)$$

and

$$\mathbf{v}_b = \left(\frac{\partial}{\partial t} \xi_{bx}, \frac{\partial}{\partial t} \xi_{bz} \right). \quad (41)$$

In the outflow region the velocity is

$$\mathbf{v}_i = \left(v_{ix}, \frac{\partial}{\partial t} \xi_{iz} + v_{ix} \frac{\partial}{\partial x} \xi_{iz} \right). \quad (42)$$

Now we can evaluate Equation (17) in the inflow and the outflow region of both half planes and then match the solution on both sides of the shocks. For the inflow region in the upper half plane we achieve

$$\frac{\partial}{\partial t} \xi_{az} + B_a \frac{\partial}{\partial x} \xi_{az} = \frac{\partial}{\partial t} f_a + B_a \frac{\partial}{\partial x} f_a. \quad (43)$$

The solution of this equation is obvious

$$f_a = \xi_{az} + \Phi_a(t - \frac{x}{B_a}), \quad (44)$$

where $\Phi_a(t - x/B_a)$ is an arbitrary function of its argument in the upper half plane. For the outflow region in the upper half plane we get

$$\frac{\partial}{\partial t} \xi_{iz} + B_a \frac{\partial}{\partial x} \xi_{iz} = \frac{\partial}{\partial t} f_a + B_a \frac{\partial}{\partial x} f_a, \quad (45)$$

where we used $v_{ix} - B_{ix} = B_a$. The solution we obtain is

$$f_a = \xi_{iz} - \Phi_i(t - \frac{x}{B_a}), \quad (46)$$

where Φ_i is the arbitrary function in the outflow region. Matching of equations (44, 46) leads to

$$f_a = \xi_{iz} - \Phi_i \left(t - \frac{x}{B_a} \right) = \xi_{az} + \Phi_a \left(t - \frac{x}{B_a} \right). \quad (47)$$

Similar considerations are leading to the solution for the lower half plane as

$$f_b = \xi_{iz} - \Phi_i(t + \frac{x}{B_b}) = \xi_{bz} + \Phi_b(t + \frac{x}{B_b}). \quad (48)$$

To determine the arbitrary function Φ_k with $k = a, b, i$, we consider Ohm's law with infinite conductivity in a frame of reference which is moving with the velocity \mathbf{u}

$$E_y = -[(\mathbf{v} - \mathbf{u}) \times \mathbf{B}]_y = v_{ix} B_{ix} \frac{\partial}{\partial x} \xi_{iz} - \left(\frac{\partial}{\partial t} \xi_{iz} + v_{ix} \frac{\partial}{\partial x} \xi_{iz} + \frac{\partial}{\partial t} f_{a,b} \right) B_{ix} = B_{ix} \frac{\partial}{\partial t} \Phi_k(t - x/B_{a,b}), \quad (49)$$

where $f_{a,b}$ means that we can use f_a or f_b to get the solution for region a or b , respectively. Integration gives an equation for the arbitrary function as

$$\Phi_k = \frac{1}{B_k} \int_0^t E^*(\tau) d\tau = \frac{1}{B_k} F(t), \quad (50)$$

where we defined a so-called flux function

$$F(t) = \int_0^t E^*(\tau) d\tau. \quad (51)$$

4.4 The magnetic field in the different regions

We can use equations (46) and (48) to calculate the z -components of the displacement vectors (38) and (39) at $z = 0$ as

$$\xi_{az} = \xi_{iz} - \frac{v_{ix}}{B_a} \Phi_i(t - |x|/B_a), \quad (52)$$

and

$$\xi_{bz} = \xi_{iz} + \frac{v_{ix}}{B_b} \Phi_i(t + |x|/B_b), \quad (53)$$

where we have to use absolute values of x , since we are interested in solutions along the whole x -axis. Substituting these two equations in our basic equation (34) we achieve

$$\begin{aligned} & \frac{\partial^2}{\partial t^2} \xi_{iz} - \frac{v_{ix}}{B_a} \frac{\partial^2}{\partial t^2} \Phi_i(t - |x|/B_a) - (B_a \nabla)^2 \xi_{iz} + \frac{v_{ix}}{B_a} (B_a \nabla)^2 \\ & \times \Phi_i(t - |x|/B_a) + \frac{\partial^2}{\partial t^2} \xi_{iz} + \frac{v_{ix}}{B_b} \frac{\partial^2}{\partial t^2} \Phi_i(t + |x|/B_b) - \\ & - (B_b \nabla)^2 \xi_{iz} - \frac{v_{ix}}{B_b} (B_b \nabla)^2 \Phi_i(t + |x|/B_b) = 0. \end{aligned} \quad (54)$$

This equation can be rewritten as

$$\left[\frac{\partial^2}{\partial t^2} - \left(\frac{B_a^2 + B_b^2}{2} \right) \frac{\partial^2}{\partial x^2} \right] \xi_{iz} = 2\Phi_i'(t) v_{ix} \delta(x), \quad (55)$$

where $\delta(x)$ is the Dirac function, and prime means derivation with respect to the argument. The Dirac function results from the second derivative of the absolute value of x , since

$$\frac{\partial}{\partial x} |x| = \text{sgn}(x),$$

and

$$\frac{\partial}{\partial x} \text{sgn}(x) = 2\delta(x).$$

The solution of Equation (55) is found to be

$$\xi_{iz} = \frac{v_{ix}}{c} \Phi_i(t - |x|/c), \quad (56)$$

where

$$c = \sqrt{\frac{B_a^2 + B_b^2}{2}}.$$

This gives the boundary conditions for the magnetic field components at $z = 0$ in the two inflow and the outflow region as

$$B_{az0} = B_a \frac{\partial}{\partial x} \xi_{az} = \frac{B_a v_{ix}}{c^2 B_{ix}} E^*(t - |x|/c) \text{sgn}(x) - \frac{v_{ix}}{B_a B_{ix}} E^*(t - |x|/B_a) \text{sgn}(x), \quad (57)$$

$$B_{bz0} = B_b \frac{\partial}{\partial x} \xi_{bz} = \frac{B_b v_{ix}}{c^2 B_{ix}} E^*(t - |x|/c) \text{sgn}(x) - \frac{v_{ix}}{B_b B_{ix}} E^*(t + |x|/B_b) \text{sgn}(x), \quad (58)$$

$$B_{iz0} = B_{ix} \frac{\partial}{\partial x} \xi_{iz} = \frac{v_{ix}}{c^2} E^*(t - |x|/c) \text{sgn}(x), \quad (59)$$

where E^* is the reconnection electric field, which is a function of its argument. These three equations are the Dirichlet boundary conditions needed to solve the Laplace equation for the B_z component, which follows directly from the arguments in Appendix A, to get the magnetic field configuration in the whole space. The solution of the Dirichlet problem in the upper half plane is given by the Poisson integral [34] for the x - and z -components of the perturbed magnetic field

$$B_{ax} = \frac{1}{\pi} \int_{-t}^{+t} \frac{(x - \xi) B_{az0} d\xi}{(x - \xi)^2 + z^2}, \quad (60)$$

and

$$B_{az} = \frac{z}{\pi} \int_{-t}^{+t} \frac{B_{az0} d\xi}{(x - \xi)^2 + z^2}. \quad (61)$$

For the lower half plane, similar expressions can be found. An example for the solution is shown in Figure 2.

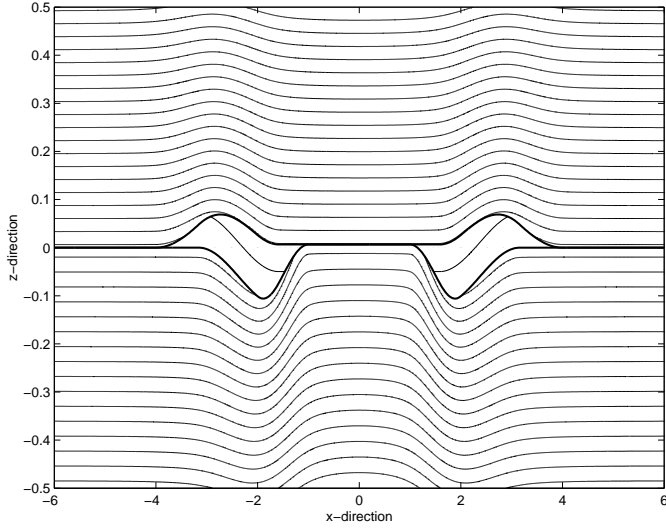


Figure 2: Asymmetric reconnection for $B_a = 2$ and $B_b = -1$ at $t = 2$. The thick lines indicate the shape of the shocks and the discontinuity, while the thin ones represent the magnetic field configuration.

5 DETERMINATION OF THE MAGNETIC FIELD ALONG A PROFILE

In principle, the magnetic field along a profile can be evaluated from the Poisson integrals (60, 61), but for the computational treatment of the problem and for solving the inverse problem is to calculate the Fourier transform of the magnetic field at the reconnection line and solve the problem in Fourier space. It is convenient to use the discrete transform because our data are given as a series with N samples of the form $x_0, x_1, x_2, \dots, x_{N-1}$. The Fourier transform of this series will be denoted $X(k)$, it will also have N samples. The forward transform will be defined as [35]

$$X(n) = \frac{1}{N} \sum_{k=1}^N x(k) e^{-i \frac{2\pi(k-1)(n-1)}{N}}, \quad (62)$$

whereas the inverse transform is defined as

$$x(n) = \sum_{k=1}^N X(k) e^{i \frac{2\pi(k-1)(n-1)}{N}}. \quad (63)$$

For our purpose it is necessary to know the derivation of a discrete Fourier transform

$$\frac{d}{dx} f = \frac{f(x + \Delta x) - f(x)}{\Delta x} = \frac{f(n+1) - f(n-1)}{2\Delta x},$$

with

$$f(n+1) = \frac{1}{N} \sum X(k) e^{i \frac{2\pi(k-1)n}{N}}$$

and

$$f(n-1) = \frac{1}{N} \sum X(k) e^{i \frac{2\pi(k-1)(n-2)}{N}}.$$

Now we can evaluate

$$\begin{aligned} \frac{f(n+1) - f(n-1)}{2\Delta x} &= \frac{1}{N} \sum X(k) e^{i \frac{2\pi(k-1)(n-1)}{N}} \\ &\quad \times \frac{i}{\Delta x} \sin \frac{2\pi(k-1)}{N}. \end{aligned} \quad (64)$$

Comparison with Equation (63) shows that the derivative of the DFT can be written as

$$\frac{\partial}{\partial x} \equiv \frac{i}{\Delta x} \sin \frac{2\pi(k-1)}{N}. \quad (65)$$

In the same way we can write

$$\frac{d^2 f}{dx^2} = \frac{f(n+1) - 2f(n) + f(n-1)}{(\Delta x)^2}$$

and we get

$$\frac{\partial^2}{\partial x^2} \equiv \frac{-4}{(\Delta x)^2} \sin^2 \frac{\pi(k-1)}{N}. \quad (66)$$

In the inflow region we can introduce a scalar potential, which satisfies the Laplace equation (compare with Appendix A)

$$\Delta \phi = 0. \quad (67)$$

By using Equation (66) the Laplace equation for the scalar potential can be written as

$$\frac{\partial^2 \phi(k)}{\partial z^2} - \frac{4}{(\Delta x)^2} \sin^2 \frac{\pi(k-1)}{N} \phi(k) = 0, \quad (68)$$

where $\phi(k)$ means the Fourier transform of ϕ . If we substitute

$$\gamma^2 = \frac{4}{(\Delta x)^2} \sin^2 \frac{\pi(k-1)}{N},$$

the general solution of Equation (68) is

$$\phi(k) = c_1 e^{|\gamma|z} + c_2 e^{-|\gamma|z}. \quad (69)$$

Since we do not want our solution to go to infinity, we assume $c_1 = 0$. For determining the second integration constant c_2 , we can use the fact that the Fourier transform of ϕ along the x -axis ($z = 0$) is $\phi_0(k)$, and it follows $c_2 = \phi_0(k)$. The solution we achieve is

$$\phi(k) = \phi_0(k) e^{-|\gamma|z}. \quad (70)$$

To get the magnetic field we use $B_z|_{z=0} = \frac{\partial \phi}{\partial z}|_{z=0} = f$ and $\phi(k) = c e^{-\gamma z}$, which gives

$$\frac{\partial \phi(k)}{\partial z} = -\gamma c e^{-\gamma z}.$$

For $z = 0$ we get $-\gamma c = f(k)$, which gives

$$\phi(k) = -\frac{f(k)}{\gamma} e^{-\gamma z}. \quad (71)$$

Differentiation with respect to z leads to

$$B_z(k) = f(k) e^{-\gamma z} = B_{z0}(k) e^{-\gamma z}. \quad (72)$$

The solution for a certain value of z is obtained by using the inverse Fourier transform

$$B_z(x) = \mathcal{F}^{-1} B_z(k). \quad (73)$$

The same calculations can be done for the x -component of the magnetic field. As expected, both methods achieve the same results, but the Fourier method can be computed much faster, since the FFT algorithms are working faster than the numerical solution of the Poisson integral. In Figure 3, the magnetic field components are plotted, showing the behaviour expected for flux transfer events.

6 THE INVERSE PROBLEM

Inverse problems are well-known in many fields of science and technology, for example in astrophysics, plasma diagnostics or tomography [36]. In principle, an inverse problem can be seen as a model of a phenomenon characterized by ζ , which belongs to a certain space of models Z . Furthermore, let u be the observed indirect attributes of

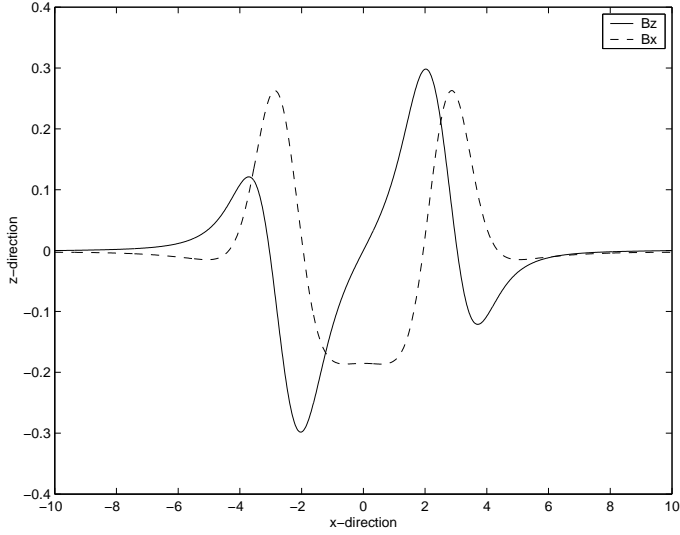


Figure 3: The magnetic field components along $z = 1$. One can see the bipolar variation of the z -component and the deflection of the x -component, as expected for FTEs.

the phenomenon with $u \in U$. An operator A relates the two values by

$$A\zeta = u.$$

As a rule, the ζ attributes cannot be directly observed. The main job when solving an inverse problem is to find out, whether the chosen model is compatible with the experimental data. The mathematical difficulty of solving such problems is that the inverse operator A^{-1} defined throughout its domain $AZ \subset U$ is not continuous. Hence there is the conventional division into the classes of well-posed and ill-posed problems. A well-posed problem, as defined by Hadamard [37], must meet the requirements that:

1. equation $A\zeta = u$ is solvable for the entire space U ,
2. the solution is unique,
3. the solution is stable, meaning that small perturbations of u result in small perturbations of the solution.

For ill-posed problems, requirements 1 and 3 are not fulfilled. These kind of problems can be solved by using the theory of regularisation [16], which we apply in the following.

Our aim is to restore the magnetic field configuration along the x -axis out of a the configuration along a certain trajectory. For this purpose, we can use Equation (72) to get the magnetic field along the x -axis, which gives

$$B_{z0}(k) = B_z(k)e^{\gamma z}. \quad (74)$$

To avoid that our solution goes to infinity for large values of γz , we use

$$B_{z0}(k) = \frac{B_z(k)}{e^{-\gamma z} + M}. \quad (75)$$

This method is called regularisation and M is referred to as regularisation operator, which is used to avoid that the denominator goes to zero for large values of γz . In this case, we use $M = \text{const}$. It is easy to see that this is an ill-posed problem, since requirement 1 is not fulfilled, if the denominator goes to zero without using the regularisation parameter. Requirement 3 is not fulfilled, if the denominator is close to zero, where small perturbations of $B_z(k)$ cause large changes in the solution. We have determined the regularisation parameter by comparing the reconnection rate for the initial magnetic field configuration with the reconnection rate for the restored magnetic field configuration, which can be seen in Figure 4.

We found that the regularisation parameter lies between 10^{-8} and 10^{-9} for small distances ($z = 0.1 - 1$) away from the reconnection

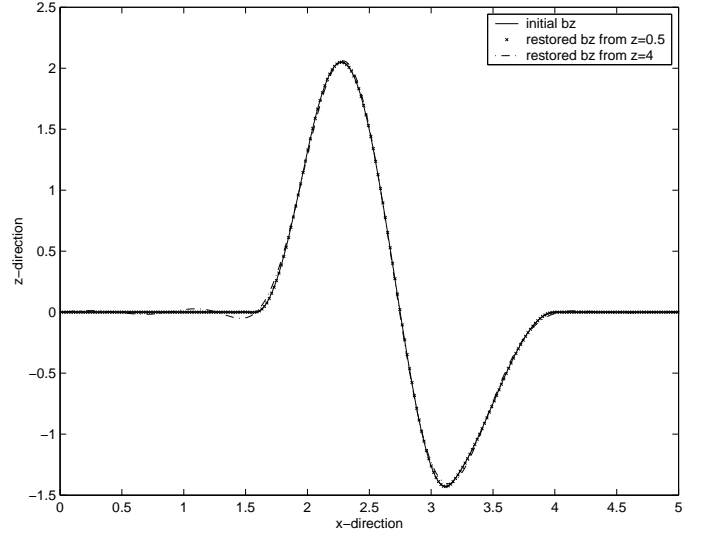


Figure 4: The initial magnetic field component (solid line) and the restored magnetic field for different distances above the reconnection site.

site, and decreases to $10^{-14} - 10^{-16}$ for distances of about 50 times the height of the field reversal region ($z > 4$). For small distances, the initial magnetic field can be restored nearly exactly, while for larger distances oscillations appear for the restored magnetic field (Figure 4).

To reconstruct the reconnection electric field, we developed an iteration method based on Equation (57), which can be written as

$$B_{az} = c_1 E^*(t - x/c) - c_2 E^*(t - x/B_a), \quad (76)$$

where we consider only $x > 0$ and $c_1 = B_a v_{ix}/(c^2 B_{ix})$ and $c_2 = v_{ix}/(B_a B_{ix})$. If we assume $|B_a| > |B_b|$, it follows that $B_a > c$. Having in mind that the electric field is zero for $\arg(E^*) < 0$, it follows that in the range

$$ct < x < B_a t, \quad (77)$$

the electric field

$$E^*(t - x/c) = 0, \quad (78)$$

while $E^*(t - x/B_a)$ has a certain value. We can apply a variable transformation

$$\tau = t - \frac{x}{B_a}, \quad (79)$$

and get the electric field in the range mentioned above as

$$E^*(\tau) = -\frac{1}{c_2} B_{az}(B_a(t - \tau)). \quad (80)$$

After interpolating $E^*(\tau)$ from steps $t - x/B_a$ to steps $t - x/c$, we get the values for $E^*(t - x/c)$, which we rename as $\hat{E}^*(\tau)$. This electric field can now be introduced into Equation (76) to get the electric field for the next interval as

$$E^*(\tau) = \frac{1}{c_2} \left(c_1 \hat{E}^*(\tau) - B_{az}(B_a(t - \tau)) \right). \quad (81)$$

This procedure can be repeated as often as necessary to reestablish the whole electrical field. This method works good, if the magnetic field strength in the upper and the lower half plane are strongly asymmetric, because in this case, we do not need many iteration steps. But if the magnetic fields are nearly symmetric, many iteration steps are needed and the solution is not satisfying anymore. A second disadvantage of the method is that it does not work good for distances larger than $z = 3$ above the reconnection line, since the oscillations appearing in the reconstructed magnetic field influence the iteration method. Both effects together are shown in Figure 6. Additionally, this method is not realistic since for measuring a profile it would be necessary to have many satellites, which make their measurements simultaneously along a profile.

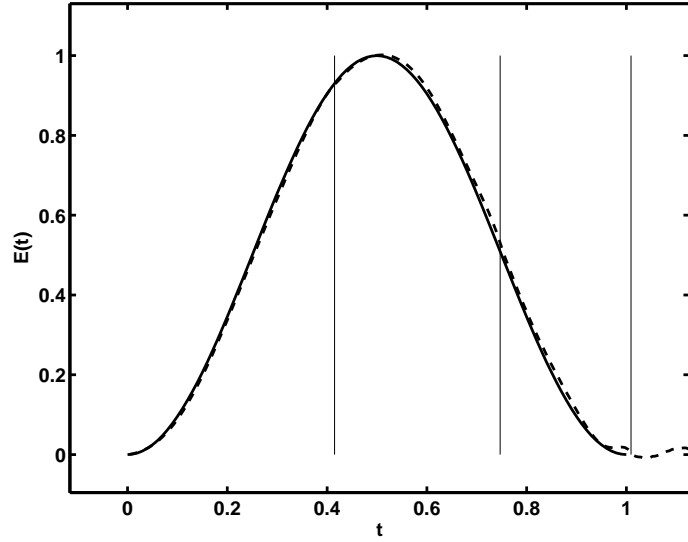


Figure 5: The initial (solid line) and the reconstructed electric field (dashed line) for $B_a = 2$ and $B_b = -1$ at $z = 1$. The thin vertical lines indicate the iteration steps. In this case, only three iteration steps were necessary.

7 THE CAGNIARD–DEHOOP METHOD FOR INCOMPRESSIBLE PLASMA

7.1 The displacement vector in \mathcal{L} – \mathcal{F} space

To calculate the magnetic field components along a trajectory $B_z(t)$, we use the so-called Cagniard–deHoop method [17, 18, 19] which is used in seismology to describe elastic waves. The method was applied to reconnection problems by Heyn and Semenov [20] and by Semenov *et al.* [38] for compressible plasma. This method will give us the magnetic field components as a convolution integral, which can be treated convenient in the theory of inverse problems [16].

Our starting point is the linearized equation of motion (25). If we apply a Laplace transformation \mathcal{L} with respect to time and a Fourier transformation \mathcal{F} with respect to the space coordinate x , we can substitute

$$\frac{\partial}{\partial t} f(x, z, t) \rightarrow p f(x, z, p), \quad (82)$$

and

$$\frac{\partial}{\partial x} f(x, z, t) \rightarrow i k f(k, z, t). \quad (83)$$

Applying \mathcal{L} and \mathcal{F} on the z -component of (25) gives

$$(p + v_0 i k) \mathbf{v}(k, z, p) = -\frac{\partial P}{\partial z} + B_0 i k \mathbf{B}(k, z, p). \quad (84)$$

Now we can introduce the displacement vector (23, 24) in Equation (84) leading to

$$(p + v_0 i k)^2 \xi = -\frac{\partial P}{\partial z} + (B_0 i k)^2 \xi. \quad (85)$$

It can be shown that the z -component of the displacement vector fulfills the Laplace equation (see Appendix A), giving

$$\frac{\partial^2 \xi_z}{\partial z^2} + k^2 \xi_z = 0 \quad (86)$$

in \mathcal{L} – \mathcal{F} space. It is obvious that this equation is similar to Equation (68) which we used in the Fourier method. Solutions of this equation can be written as

$$\xi_{az} = c_a e^{-|k|z} \quad \forall z > 0, \quad (87)$$

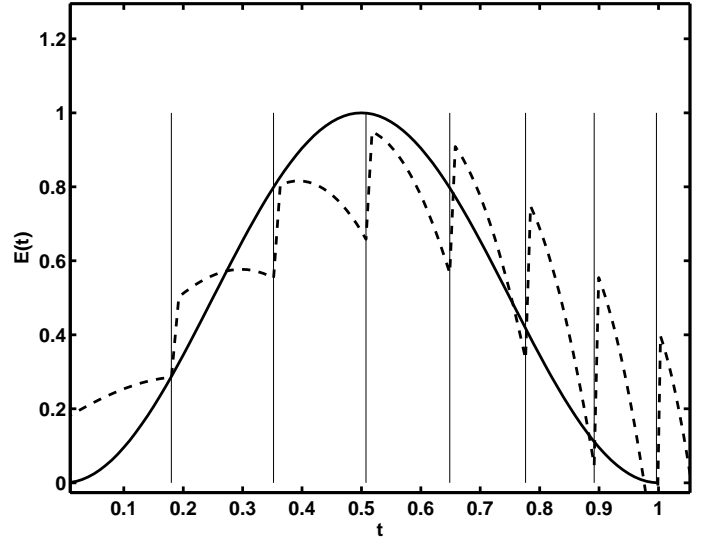


Figure 6: The initial (solid line) and the reconstructed electric field (dashed line) for $B_a = 2$ and $B_b = -1.6$ at $z = 5$. The thin vertical lines indicate the iteration steps.

and

$$\xi_{bz} = c_b e^{|k|z} \quad \forall z < 0. \quad (88)$$

Inserting equations (87, 88) into (85) for $v_0 = 0$ leads to

$$\frac{\partial P_a}{\partial z} = -\epsilon_a \xi_{az} = -\epsilon_a c_a e^{-|k|z}, \quad (89)$$

in the upper half plane, and

$$\frac{\partial P_b}{\partial z} = -\epsilon_b \xi_{bz} = -\epsilon_b c_b e^{|k|z}, \quad (90)$$

in the lower half plane, where we use $\epsilon = p^2 + B_0^2 k^2$. Integration of equations (89, 90) and using the total pressure balance $P_a = P_b$ gives the dispersion relation at $z = 0$ as

$$\epsilon_a c_a + \epsilon_b c_b = 0. \quad (91)$$

At $z = 0$, we can define a source term in \mathcal{L} – \mathcal{F} space as

$$Q(k, p) = \xi_{az} - \xi_{bz} = c_a - c_b. \quad (92)$$

Inserting this source term in equations (87, 88), respectively, gives the displacement vector in \mathcal{L} – \mathcal{F} space as

$$\xi_{az}(k, p) = \frac{\epsilon_b}{\epsilon_a + \epsilon_b} Q(k, p) e^{-|k|z}, \quad (93)$$

in the upper half plane, and

$$\xi_{bz}(k, p) = -\frac{\epsilon_a}{\epsilon_a + \epsilon_b} Q(k, p) e^{|k|z}, \quad (94)$$

in the lower half plane.

7.2 The source term in \mathcal{L} – \mathcal{F} space

Now we have to determine the source term in \mathcal{L} – \mathcal{F} space. Therefore, we start with the known shape of the shocks in real space f_a and f_b from equations (47, 48). Subtracting Equation (48) from Equation (47), we get the source term in real space as

$$Q(x, t) = \xi_{az}(x, t) - \xi_{bz}(x, t) = \Phi_i(t - |x|/B_a) - \Phi_i(t + |x|/B_b) + \Phi_b(t + |x|/B_b) - \Phi_a(t - |x|/B_a). \quad (95)$$

Now we apply \mathcal{L} and \mathcal{F} to the first term on the right hand side of Equation (95) yielding

$$Q^{(1)}(p, k) = \int_0^\infty dt e^{-pt} \int_{-\infty}^\infty dx e^{-ikx} \Phi_i(t - |x|/B_a) = \frac{2pB_a}{B_{ix}(p^2 + B_a^2k^2)} F(p), \quad (96)$$

where $F(p)$ is the reconnected flux in \mathcal{L} space. Here we use a variable transformation $\tau = t - |x|/B_a$ and the condition of causality

$$\Phi_k(x) \equiv 0 \quad \forall x < 0. \quad (97)$$

For the other three terms on the right hand side of Equation (95) similar expressions can be achieved. Therefore, we can write the whole source term (95) in \mathcal{L} - \mathcal{F} space as

$$Q(p, k) = \frac{2p}{B_{ix}} \left(\frac{B_a - B_{ix}}{p^2 + k^2 B_a^2} + \frac{B_b - B_{ix}}{p^2 + k^2 B_b^2} \right) F(p) = \frac{2p v_{ix}}{B_{ix}} \left(\frac{1}{p^2 + k^2 B_a^2} - \frac{1}{p^2 + k^2 B_b^2} \right) F(p), \quad (98)$$

where we used $v_{ix} = (B_a - B_{ix})/2$. Additionally, we can evaluate

$$\epsilon_a + \epsilon_b = 2(p^2 + c^2 k^2), \quad (99)$$

with $c^2 = (B_a^2 + B_b^2)/2$ as the velocity of surface waves, similar as in Section 3. Inserting equations (98) and (99) into equation (93, 94) gives the displacement vector in the upper and the lower half plane as

$$\xi_{az, bz}(k, z, p) = \pm \frac{p v_{ix}(p^2 + k^2 B_{b,a}^2)}{B_{ix}(p^2 + c^2 k^2)} \times \left(\frac{1}{p^2 + k^2 B_a^2} - \frac{1}{p^2 + k^2 B_b^2} \right) F(p) e^{\mp |k|z}. \quad (100)$$

7.3 The displacement vector in real space

To get the displacement vector in real space, we apply an inverse Fourier transformation \mathcal{F}^{-1} to Equation (100) giving

$$\xi_{az}(x, z, p) = \frac{v_{ix}}{2\pi B_{ix}} \int_{-\infty}^\infty \frac{p^2 + k^2 B_b^2}{p^2 + c^2 k^2} \times \left(\frac{1}{p^2 + k^2 B_a^2} - \frac{1}{p^2 + k^2 B_b^2} \right) p F(p) e^{-|k|z} e^{ikx} dk. \quad (101)$$

Performing a variable transformation $k = sp$ leads to

$$\xi_{az}(x, z, p) = \frac{v_{ix}}{2\pi B_{ix}} \int_{-\infty}^\infty K(s) F(p) e^{-|ps|z} e^{ispx} ds, \quad (102)$$

with

$$K(s) = \frac{1 + s^2 B_b^2}{1 + c^2 s^2} \left(\frac{1}{1 + s^2 B_a^2} - \frac{1}{1 + s^2 B_b^2} \right). \quad (103)$$

After a second variable transformation $s \rightarrow -s$, the argument of the integral in Equation (102) becomes the complex conjugate, and therefore we can replace the integration

$$\int_{-\infty}^\infty \rightarrow 2 \Re \int_0^\infty.$$

Now we achieve

$$\xi_{az}(x, z, p) = \frac{v_{ix}}{\pi B_{ix}} \Re \int_0^\infty K(s) F(p) e^{-p\tau(s)} ds, \quad (104)$$

with

$$\tau(s) = sz - isx. \quad (105)$$

The argument of the integral in Equation (104) has the same form like the shift theorem for the Laplace transformation

$$\mathcal{L}(\Phi(t - a)) = e^{-pa} \hat{\Phi}(p) \quad \text{for } a \in \mathbb{R}. \quad (106)$$

In our case, it is obvious that $\tau(s) \in \mathbb{C}$, but we can use the Cauchy theorem to transform $\tau(s)$ to a curve, where $\Im(\tau(s)) = 0$. Cauchy theorem proposes that if \mathcal{C} is a closed path lying within a region, where $f(z)$ is analytic, meaning that there are no poles inside this region, then

$$\oint_{\mathcal{C}} f(z) dz = 0. \quad (107)$$

Now we can construct a closed path, which is shown in Figure 7, where \mathcal{C}_1 represents the integration from 0 to infinity. It is possible

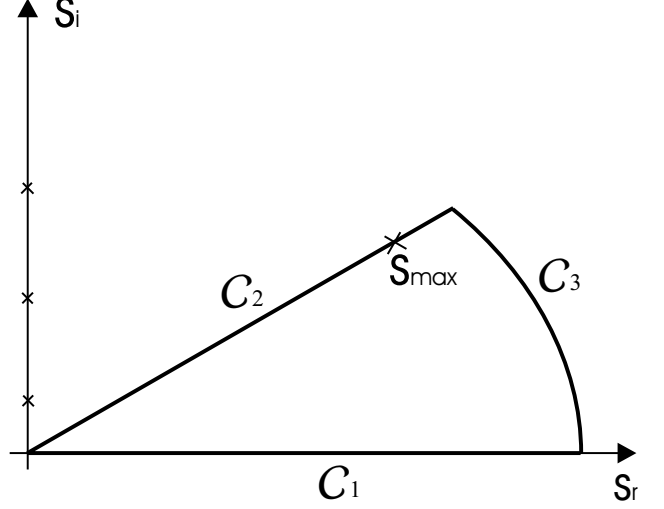


Figure 7: The closed path for the evaluation of the Cauchy theorem. The crosses indicate that the poles are located along the imaginary axis.

to define a curve, where $\Im(\tau(s)) \equiv 0$. Substituting $s = s_r + i s_i$ gives

$$\Im(-i(s_r + i s_i)x + (s_r + i s_i)z) = 0, \quad (108)$$

which leads to

$$\frac{s_i}{s_r} = \frac{x}{z}. \quad (109)$$

This integration path is represented by \mathcal{C}_2 in Figure 7. It can be shown that $\Re(\tau(s)) > 0$ along \mathcal{C}_3 , and therefore this integral is decreasing exponentially and can be neglected. Due to Equation (107), we can replace the integration along \mathcal{C}_1 by an integration along \mathcal{C}_2 , where $\Im(\tau(s)) = 0$.

After application of an inverse Laplace transformation \mathcal{L}^{-1} , Equation (104) can be written as

$$\xi_{az}(x, z, t) = \frac{v_{ix}}{\pi B_{ix}} \Re \int_{\mathcal{C}_2} K(s) \times \frac{1}{2\pi i} \int_{\sigma - i\infty}^{\sigma + i\infty} F(p) e^{-p\tau(s)} e^{pt} dp ds, \quad (110)$$

where σ is large enough that $f(x, z, p)$ is defined for $\Re(p) \geq \sigma$. Since $\tau(s) \in \mathbb{R}$, we can use the shift theorem for Laplace transformations (106) and get

$$\xi_{az}(x, z, t) = \frac{v_{ix}}{\pi B_{ix}} \Re \int_{\mathcal{C}_2} K(s) F(t - \tau(s)) ds. \quad (111)$$

Due to the condition of causality (97), $F(t - \tau(s)) \equiv 0$ if $t - \tau(s) \leq 0$. Therefore, we can define an upper limit s_{max} (Figure 7) for the integration along \mathcal{C}_2 when $t = \tau(s)$. After performing a variable transformation $s \rightarrow \tau$, we get the displacement vector in real space as the convolution integral

$$\xi_{az}(x, z, t) = \frac{v_{ix}}{\pi B_{ix}} \Re \int_0^t g_a(x, z, \tau) F(t - \tau) \frac{1}{q_a(x, z)} d\tau, \quad (112)$$

with

$$g_a(x, z, \tau) = \frac{q_a^2 + B_b^2 \tau^2}{q_a^2 + c^2 \tau^2} \left(\frac{q_a^2}{q_a^2 + B_a^2 \tau^2} - \frac{q_a^2}{q_a^2 + B_b^2 \tau^2} \right), \quad (113)$$

and

$$q_a(x, z) = z - i x. \quad (114)$$

The same arguments give the displacement vector in the lower half plane as

$$\xi_{bz}(x, z, t) = -\frac{v_{ix}}{\pi B_{ix}} \Re \int_0^t g_b(x, z, \kappa) F(t - \kappa) \frac{1}{q_b(x, z)} d\kappa, \quad (115)$$

with

$$g_b(x, z, \kappa) = \frac{q_b^2 + B_a^2 \kappa^2}{q_b^2 + c^2 \kappa^2} \left(\frac{q_b^2}{q_b^2 + B_a^2 \kappa^2} - \frac{q_b^2}{q_b^2 + B_b^2 \kappa^2} \right), \quad (116)$$

and

$$q_b(x, z) = -z - i x. \quad (117)$$

7.4 Evaluation of the magnetic field configuration

To calculate the z -component of the magnetic field, we use that

$$B_{az} = B_a \frac{\partial}{\partial x} \xi_{az}. \quad (118)$$

It is convenient to perform the spatial derivation in the \mathcal{L} - \mathcal{F} space, so that we can insert Equation (102) into Equation (118), yielding

$$B_{az} = \frac{v_{ix} B_a}{2\pi B_{ix}} \int_{-\infty}^{\infty} K(s) F(p) i s p e^{-|p s|z} e^{i s p x} ds. \quad (119)$$

In Laplace space the reconnection electric field can be written as $E(p) = p F(p)$, which gives the z -component of the magnetic field as

$$B_{az}(x, z, t) = \frac{v_{ix} B_a}{\pi B_{ix}} \Re \int_0^t g_a(x, z, \tau) E(t - \tau) \frac{i \tau}{q_a(x, z)^2} d\tau. \quad (120)$$

The x -component of the magnetic field can be determined by using the definition of the displacement vector (23), which gives for the x -component

$$B_{ax} = B_a \frac{\partial}{\partial x} \xi_{ax}. \quad (121)$$

If we use Equation (7), we can write Equation (121) as

$$B_{ax} = -B_a \frac{\partial}{\partial z} \xi_{az}. \quad (122)$$

If we solve this equation in \mathcal{L} - \mathcal{F} space, we get the x -component of the magnetic as

$$B_{ax}(x, z, t) = \frac{v_{ix} B_a}{\pi B_{ix}} \Re \int_0^t g_a(x, z, \tau) E(t - \tau) \frac{\tau}{q_a(x, z)^2} d\tau. \quad (123)$$

The calculated profiles are equivalent to the profiles calculated by using the Fourier method (Figure 3).

In the upper half plane similar expressions for the magnetic field components can be achieved.

8 RECONSTRUCTION OF THE RECONNECTION RATE

8.1 The inverse problem for the Cagniard–deHoop method

In nature, the shocks are moving with velocities of some hundred km/s, while the satellite's velocity is only some km/s. Therefore,

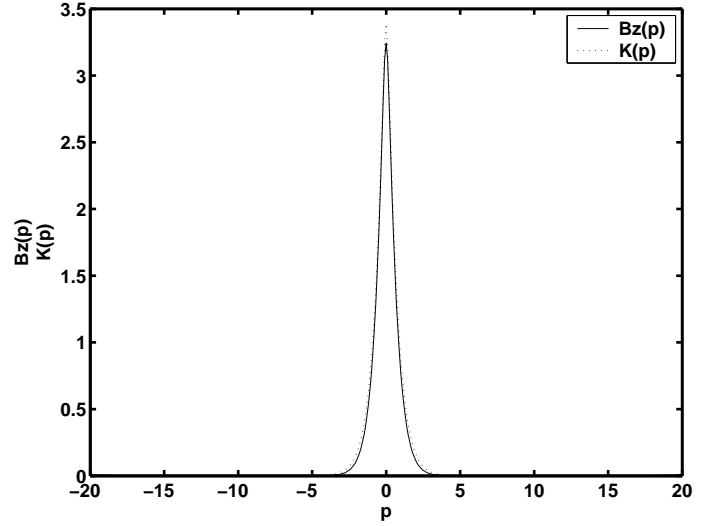


Figure 8: $K(p)$ and $B_z(p)$ in Laplace space.

we can consider the satellite as fixed, meaning that $x = const$ and $z = const$ in this case. Now the magnetic field is only a function of time $B_z(x, z, t) \equiv B_z(t)$. Our starting point is the convolution integral for the z -component of the magnetic field (120) for a fixed position in space. In Laplace space, the convolution integral can be written as

$$B_z(p) = K(p)E(p), \quad (124)$$

which is similar to Equation (74) in the Fourier method. From Equation (124) it looks quite simple to reconstruct the reconnection electric field as

$$E(p) = \frac{B_z(p)}{K(p)}. \quad (125)$$

If we visualize both functions $K(p)$ and $B_z(p)$ (Figure 8), we see that for large absolute values of z we divide very small numbers. This leads to large oscillations in the result, which is a characteristic feature for ill-posed inverse problems. To avoid this oscillating function (Figure 9), we introduce again a regularisation operator $M(p)$ in Equation (125) giving

$$E(p) = \frac{B_z(p)}{K(p) + M(p)}. \quad (126)$$

The regularisation operator $M(p)$ is defined as

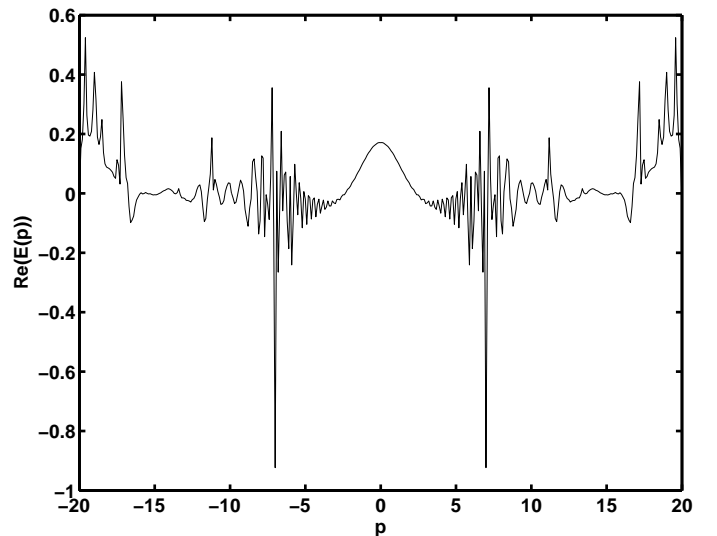


Figure 9: The real part of the reconnection electric field without regularisation. In this case, $R_{max} \approx 4$.

$$M(p) = \begin{cases} 0 & |p| < R_{max} \\ \infty & |p| > R_{max} \end{cases}. \quad (127)$$

This operator does not influence the electric field for small values of p , where the two functions are not small. But when the functions reach small values ($p > R_{max}$), the denominator goes to infinity, so that the reconnection electric field is zero in Laplace space and large oscillations are suppressed. The value of R_{max} can be found intuitively by deciding where the oscillations are becoming too large.

8.2 Reconstruction of an exponential reconnection electric field

At first, we use an initial electric field of the form

$$E(t) = \frac{b^2 e^2}{20} t^2 e^{-bt}, \quad (128)$$

with $b = 4$. We can use the magnetic field trajectories obtained via the Cagniard–deHoop method to reconstruct the electric field. If we use a magnetic field configuration with $B_a = 2$ and $B_b = -1$ and reconstruct the electric field from a satellite position at $x = 5$ and $z = 2$ the result is very satisfying (Figure 10). The coincidence

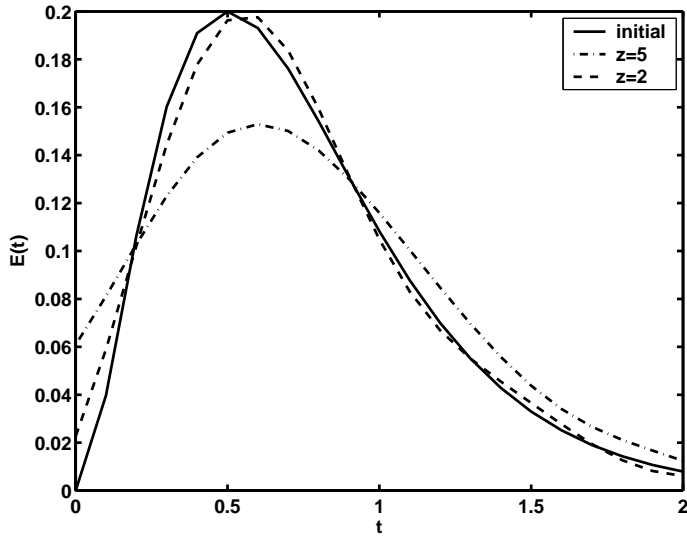


Figure 10: Reconstructed and initial electric field for a position $x = 5$ and $z = 2$ (dotted line) and $z = 5$ (dashed-dotted line) for a magnetic field configuration $B_a = 2$ and $B_b = -1$.

between the initial and the reconstructed electric field is good and only small oscillations occur. The value of R_{max} is chosen to be 7.5 in this case. For a larger distance of the satellite above the reconnection site of $z = 5$ the agreement is still qualitatively good with $R_{max} = 5$. From Figure 2 it can be seen that the outflow region has a size of approximately 0.1 in z -direction. Therefore, this remote sensing method works good for distances up to more than 50 times the height of the outflow region. This shows that the assumption of weak reconnection is justified since it leads to a thin outflow region, but also in this case it works for quite large absolute distances. For larger distances above the reconnection site the agreement is getting worse. The value of x does not influence the agreement significantly. Now we can vary the magnetic field configuration. The situation for $B_a = 5$ and $B_b = -1$ is shown in Figure 11. For a distance of $z = 2$ we use $R = 10$ and can reconstruct the electric field very good. For a larger distance of $z = 5$ and $R = 5$ the electric field can be restored better than for a magnetic field of $B_a = 2$. Also for a magnetic field configuration of $B_a = 5$ and $B_b = -4$, the reconstruction method works very good.

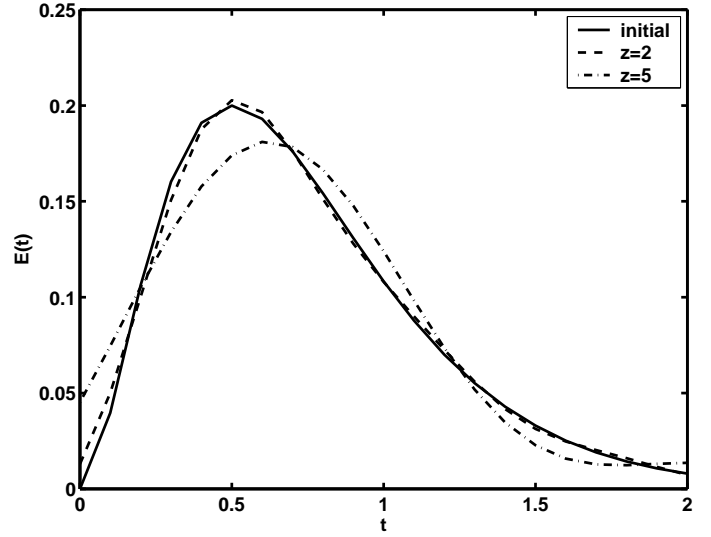


Figure 11: Same as Figure 10, but for a magnetic field configuration $B_a = 5$ and $B_b = -1$.

8.3 Reconstruction of sine-shaped electric fields

In this case, we use an initial electric field as

$$E(t) = \begin{cases} \sin^2(\pi t) & 0 \leq t \leq 1 \\ 0 & \text{else} \end{cases}. \quad (129)$$

The reconstructed electric field for a magnetic field configuration of $B_a = 2$ and $B_b = -1$ is shown in Figure 12. For a distance of $z = 2$ above the reconnection site the agreement is quite good by using $R = 10$, but for $z = 5$ the coincidence is worse than for an exponential electric field since the sine pulse is not as smooth as the exponential function. For a larger magnetic field in the upper half plane $B_a = 5$, the initial magnetic field can be reconstructed very well also for a distance of $z = 5$. Additionally, we can model the

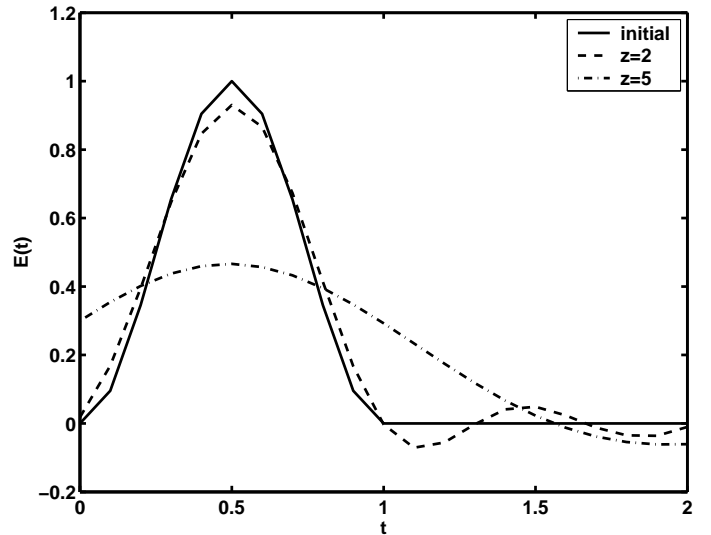


Figure 12: Reconstructed and initial electric field for a sine-shaped electric field for $B_a = 2$ and $B_b = -1$ for a distance of $z = 2$ (dotted line) and $z = 5$ (dashed-dotted line).

case of two reconnection pulses. Here we use a initial reconnection electric field of the form

$$E(t) = \begin{cases} \sin^2(\pi t) & 0 \leq t \leq 1 \quad \text{and} \quad 2 \leq t \leq 3 \\ 0 & \text{else} \end{cases}. \quad (130)$$

If we apply our reconstruction method to such a electric field, we can reconstruct the electric field for $z = 2$ very good and for $z = 5$ qualitatively good (Figure 13) for a magnetic field $B_a = 2$ and $B_b = -1$. The used values for R are 15 for $z = 2$ and 7.5 for $z = 5$. As in

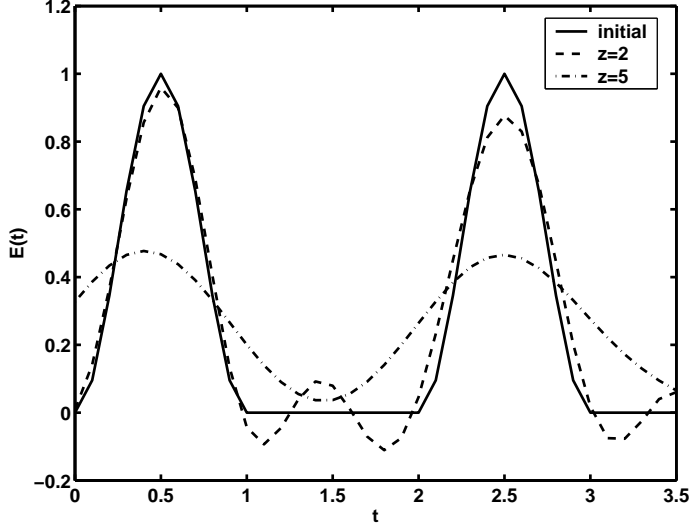


Figure 13: Reconstructed and initial electric field two sine-shaped reconstruction pulses for $B_a = 2$ and $B_b = -1$ for a distance of $z = 2$ (dotted line) and $z = 5$ (dashed-dotted line).

the previous cases, the magnetic field configuration of $B_a = 5$ and $B_b = -1$ enables us to reconstruct the electric field better than for $B_a = 2$. If the time separation of the pulses is larger, the method works similar than for single pulses. For large distances and small time separation it is not possible to reconstruct the right structure from the magnetic field profiles since they are not clearly separated at large distances above the reconnection site.

9 CONCLUSION

In this article, we presented a new method for the reconstruction of the reconnection rate from disturbances in the ambient magnetic field, which can be considered as the measurements of a hypothetical satellite. First, the magnetic field components at the reconnection site are determined from a profile. The convolution integral for this case is given as a Poisson integral. A solution of the Poisson integral can be found in Fourier space rather than in Laplace space by using a regularisation method to solve the inverse problem. For this case we developed a iteration method to reconstruct the electric field for most magnetic field configurations and up to a distance of about 30 times the outflow region. But in this case we reconstruct the data from profiles, which are not realistic for satellite measurements. In a second approach, we use the Cagniard–deHoop method to calculate the magnetic field components along a trajectory. In this case, the magnetic field is given as a convolution integral, which can be solved by applying a regularisation operator. It was shown that this method gives the reconnection electric field quantitatively good for values of $z < 5$, corresponding to 50 times the height of the outflow region, and qualitatively good also for larger distances. We used different initial electric fields, and found that the method works better if the initial field has a smooth behaviour. The magnetic field configuration also influence the results in a way that a larger ratio between the magnetic fields on both sides of the discontinuity leads to a better reconstruction of the initial reconnection electric field. Also for reconnection pulses with a time separation of $t > 1$, the method works sufficiently.

APPENDIX A—Laplace equation of the displacement vector in the inflow region

To show that

$$\Delta \xi_z = 0,$$

in the inflow region, we start with the normalized equation of motion (4) and insert the definitions for the displacement vector (23, 24) getting

$$\frac{\partial^2}{\partial t^2} \xi = -\nabla P + (\mathbf{B}_0 \cdot \nabla)^2 \xi. \quad (131)$$

The x -component of this equation can be written as

$$\left(\frac{\partial^2}{\partial t^2} - \frac{\partial^2}{\partial x^2} \right) \xi_x = -\frac{\partial}{\partial x} P, \quad (132)$$

while the z -component is given as

$$\left(\frac{\partial^2}{\partial t^2} - \frac{\partial^2}{\partial x^2} \right) \xi_z = -\frac{\partial}{\partial z} P. \quad (133)$$

Differentiation of Equation (132) with respect to z , and differentiation of Equation (133) with respect to x and subtracting the latter from the first yields

$$\left(\frac{\partial^2}{\partial t^2} - \frac{\partial^2}{\partial x^2} \right) \left(\frac{\partial}{\partial z} \xi_x - \frac{\partial}{\partial x} \xi_z \right) = 0. \quad (134)$$

Here the d'Alembert operator describes the evolution of incoming slow and Alfvén waves, which may be neglected since we are considering the current free limit. Additionally, we evaluate the continuity equation for the incompressible case

$$\nabla \cdot \mathbf{v} = \frac{\partial}{\partial t} \nabla \cdot \xi = \frac{\partial}{\partial t} \left(\frac{\partial}{\partial x} \xi_x + \frac{\partial}{\partial z} \xi_z \right) = 0, \quad (135)$$

If we assume as an initial condition that

$$\nabla \cdot \xi \equiv 0 \quad \text{for } t = 0,$$

we get together with Equation (134) the Cauchy–Riemann equations

$$\frac{\partial}{\partial z} \xi_x - \frac{\partial}{\partial x} \xi_z = 0, \quad (136)$$

and

$$\frac{\partial}{\partial x} \xi_x + \frac{\partial}{\partial z} \xi_z = 0. \quad (137)$$

From the Cauchy–Riemann equations it follows directly that

$$\Delta \xi_x = \Delta \xi_z = 0. \quad (138)$$

APPENDIX B—Evaluation of the displacement vector for $z = 0$

We show that the displacement vector can be evaluated by the Cagniard–deHoop method and can be simplified to the boundary condition at $z = 0$ for the Dirichlet problem (Equation 57) by using the residue theorem. We consider the displacement vector

$$\xi_{az}(x, z, t) = \frac{v_{ix}}{\pi B_{ix}} \Re \int_c \frac{1 + s^2 B_b^2}{1 + c^2 s^2} \times \left(\frac{1}{1 + s^2 B_a^2} - \frac{1}{1 + s^2 B_b^2} \right) F(t - \tau(s)) ds, \quad (139)$$

for the case $z = 0$. For this case, $\tau = -i s x$ and we can substitute $s = i \mu$, giving

$$\xi_{az}(x, 0, t) = \frac{v_{ix}}{\pi B_{ix}} \Re \int_c \frac{1 - \mu^2 B_b^2}{1 - c^2 \mu^2} \times \left(\frac{1}{1 - \mu^2 B_a^2} - \frac{1}{1 - \mu^2 B_b^2} \right) F(t - \mu x) i d\mu. \quad (140)$$

It can be seen that the argument of the integral is purely imaginary, therefore the displacement vector at $z = 0$ should be zero. But there exist poles along the imaginary axis and we must use the residue theorem to calculate the value of the integral. The residue theorem follows from the Cauchy theorem, where we suppose that instead of an analytic function inside the contour of integration, we have a function with poles inside. Then the residue theorem says that if $f(z)$ is analytic within and on a closed contour \mathcal{C} , except for a finite number of poles n , we get

$$\oint_{\mathcal{C}} f(z) dz = 2\pi i \sum_n R(z_n). \quad (141)$$

The residue $R(z_n)$ of a single pole at z_n is defined as

$$R(z_n) = \lim_{z \rightarrow z_n} (z - z_n) f(z). \quad (142)$$

The first term on the right hand side of Equation (140) has poles at $\pm 1/c$ and $\pm 1/B_a$. In our case, we are only interested in poles along

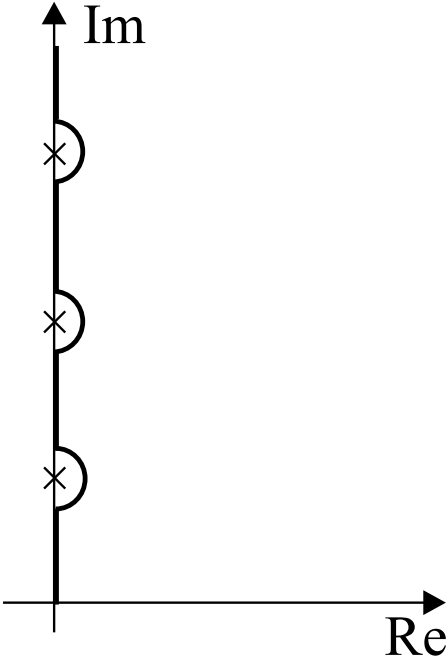


Figure 14: The path of integration is indicated by the thick line and the poles are marked by crosses. Only the half residues give a contribution for the integration.

the positive axis and can calculate the half residues (Figure 14) as

$$R^{(1)}(1/c) = \lim_{\mu \rightarrow 1/c} \left(\mu - \frac{1}{c} \right) \frac{1 - \mu^2 B_b^2}{(1 - \mu^2 c^2)(1 - \mu^2 B_a^2)} \times i F(t - \mu x) = \frac{1}{2c} \frac{c^2 + B_b^2}{c^2 - B_a^2} i F(t - x/c), \quad (143)$$

and

$$R^{(1)}(1/B_a) = \lim_{\mu \rightarrow 1/B_a} \left(\mu - \frac{1}{B_a} \right) \frac{1 - \mu^2 B_b^2}{(1 - \mu^2 c^2)(1 - \mu^2 B_a^2)} \times i F(t - \mu x) = \frac{1}{2B_a} \frac{B_a^2 - B_b^2}{B_a^2 - c^2} i F(t - x/B_a). \quad (144)$$

The second term on the right hand side of Equation (140) has poles at $\pm 1/c$ and $\pm 1/B_b$ giving residues as

$$R^{(2)}(1/c) = \lim_{\mu \rightarrow 1/c} \left(\mu - \frac{1}{c} \right) \frac{1 - \mu^2 B_b^2}{(1 - \mu^2 c^2)(1 - \mu^2 B_b^2)} \times i F(t - \mu x) = \frac{1}{2} i F(t - x/c), \quad (145)$$

and

$$R^{(2)}(1/B_b) = \lim_{\mu \rightarrow 1/B_b} \left(\mu - \frac{1}{B_b} \right) \times \frac{1 - \mu^2 B_b^2}{(1 - \mu^2 c^2)(1 - \mu^2 B_b^2)} i F(t - \mu x) = 0. \quad (146)$$

Therefore, the displacement vector can be written as

$$\xi_{az}(x, 0, t) = \frac{v_{ix}}{\pi B_{ix}} \pi i \left(R^{(1)}(1/c) + R^{(1)}(1/B_a) - R^{(2)}(1/c) \right) = \frac{v_{ix}}{2 B_{ix} c} \left(\frac{c^2 - B_b^2}{c^2 - B_a^2} - 1 \right) F(t - x/c) + \frac{v_x}{2 B_x B_a} \frac{B_a^2 - B_b^2}{B_a^2 - c^2} F(t - x/B_a). \quad (147)$$

This equation is the same as the equation used as boundary condition in the Fourier method

$$\xi_{az}(x, 0, t) = -\frac{v_{ix}}{B_{ix} c} F(t - x/c) + \frac{v_{ix}}{B_{ix} B_a} F(t - x/B_a), \quad (148)$$

to determine the magnetic field configuration as well as the shape of the shocks. This proof shows that the Cagniard–deHoop method is an equivalent method to calculate the displacement vectors and therefore all other relevant quantities.

10 ACKNOWLEDGEMENTS

This work is supported by the INTAS–ESA project 99–01277, and by the Austrian “Fonds zur Förderung der wissenschaftlichen Forschung” under projects P13804–TPH and P14744–TPH. V. S. S., I. V. K., and V. V. I. are supported by the program “Intergeophysics” from the Russian Ministry of Higher Education. V. S. S. acknowledges financial support from the Technical University Graz and the hospitality of the Institute for Theoretical Physics during a research visit to Graz. T. P. thanks the “Österreichische Forschungsgemeinschaft” for supporting a visit to the Institute of Physics of the State University in St. Petersburg. We acknowledge support by the Austrian Academy of Sciences, “Verwaltungsstelle für Auslandsbeziehungen”.

References

- [1] Russell, C. T., and Elphic, R. C. 1978, Initial ISEE magnetometer results: magnetopause observations, *Space Sci. Rev.*, 22, 681.
- [2] Biernat, H. K., Farrugia, C. J., Lawrence, G. R., Semenov, V. S., Vogl, D. F., Kiendl, M. T., Rijnbeek, R. P., and Erkaev, N. V. 2002, Flux transfer events at the magnetopause: Data aspects and theoretical approaches, *Recent Res. Devel. Plasmas*, 2, 1.
- [3] Rijnbeek, R. P., Cowley, S. W. H., Southwood, D. J., and Russell, C. T. 1982, Observations of reverse polarity flux transfer events at the Earth’s dayside magnetopause, *Nature*, 300, 23.
- [4] Southwood, D. J., Farrugia, C. J., and Saunders, M. A. 1988, What are flux transfer events?, *Planet. Space Sci.*, 36, 503.
- [5] Semenov, V. S., Kubyshkin, I. V., Lebedeva, V. V., Rijnbeek, R. P., Heyn, M. F., Biernat, H. K., and Farrugia, C. J. 1992, A comparison and review of steady–state and time–varying reconnection, *Planet. Space Sci.*, 49, 63.
- [6] Otto, A. 1991, Three–dimensional MHD computations of magnetic reconnection, in *Theoretical problems in space and fusion plasmas*, Biernat, H. K., Bauer, S. J., and Heindler, M. (eds.), Austrian Academy of Sciences, Vienna, Austria.
- [7] Southwood, D. J. 1985, Theoretical aspects of ionosphere–magnetosphere–solar wind coupling, *Adv. Space Res.*, 5, 4.

- [8] Farrugia, C. J., Elphic, R. C., Southwood, D. J., and Cowley, S. W. H. 1987, Field and flow perturbations outside the reconnected field line region in flux transfer events: theory, *Planet. Space Sci.*, 35, 737.
- [9] Walthour, D. W., Sonnerup, B. U. Ö., Paschmann, G., Lühr, H., Klumpar, D., and Potemra, T. 1993, Remote sensing of two-dimensional magnetopause structures, *J. Geophys. Res.*, 98, 1489.
- [10] Walthour, D. W., Sonnerup, B. U. Ö., Elphic, R. C., and Russell, C. T. 1994, Double vision: Remote sensing of a flux transfer event with ISEE 1 and 2, *J. Geophys. Res.*, 99, 8555.
- [11] Lawrence, G. R. 1998, MHD analysis of the solar-terrestrial interaction: Development of tools for studying magnetopause reconnection and the plasma depletion layer, Ph.D. thesis, University of Sussex, England.
- [12] Lawrence, G. R., Rijnbeek, R. P., and Semenov, V. S. 2000, Remote sensing of flux transfer events: Investigations of theoretical constraints based on model magnetopause time series data, *J. Geophys. Res.*, 105, 7629.
- [13] Hau, L.-N., and Sonnerup, B. U. Ö. 1999, Two-dimensional coherent structures in the magnetopause: Recovery of static equilibria from single-spacecraft data, *J. Geophys. Res.*, 104, 6899.
- [14] Hu, Q., and Sonnerup, B. U. Ö. 2001, Reconstruction of magnetic flux ropes in the solar wind, *Geophys. Res. Lett.*, 28, 467.
- [15] Hu, Q., and Sonnerup, B. U. Ö. 2003, Reconstruction of two-dimensional structures in the magnetopause: Method improvements, *J. Geophys. Res.*, 108, 1011, doi:10.1029/2002JA009323.
- [16] Tikhonov, A. N., and Arsenin, V. Y. 1977, Solutions of ill-posed problems, John Wiley, New York.
- [17] Lamb, H. 1904, On the propagation of tremors over the surface of an elastic solid, *Philos. Trans. R. Soc. London Ser. A*, 203, 1.
- [18] Cagniard, L. 1939, *Reflexion et Refraction des Ondes Sismiques Progressive*, Gauthier-Villard, Paris; English translation by Flinn, E. A., and Dix, C. H. 1962, *Reflection and refraction of progressive seismic waves*, McGraw-Hill, New York.
- [19] deHoop, A. T. 1960, The surface line source problem, *Appl. Sci. Res. B*, 8, 349.
- [20] Heyn, M. F., and Semenov, V. S. 1996, Rapid reconnection in compressible plasma, *Phys. Plasmas*, 3, 2725.
- [21] Heyn, M. F., Biernat, H. K., Rijnbeek, R. P., and Semenov, V. S. 1988, The structure of reconnection layers, *J. Plasma Physics*, 40, 235.
- [22] Papadopoulos, K. 1979, The role of microturbulence on collisionless reconnection, in *Dynamics of the magnetopause*, Aka-sofu, S. I. (ed.), D. Reidel Publ., Dordrecht.
- [23] Rezhnev, B. V., and Maltsev, Y. P. 1994, Role of interchange instability in flux transfer event origin, *Ann. Geophys.*, 12, 183.
- [24] Büchner, J., and Zelenyi, L. M. 1986, Deterministic chaos in the dynamics of charged particles near a magnetic field reversal, *Phys. Lett. A*, 118, 395.
- [25] Birn, J., et al. 2001, Geospace Environmental Modeling (GEM) magnetic reconnection challenge, *J. Geophys. Res.*, 106, 3715.
- [26] Shay, M. A., Drake, J. F., Rogers, B. N., and Denton, R. E. 2001, Alfvénic collisionless magnetic reconnection and the Hall term, *J. Geophys. Res.*, 106, 3759.
- [27] Biernat, H. K., Heyn, M. F., and Semenov, V. S. 1987, Unsteady Petschek reconnection, *J. Geophys. Res.*, 92, 3392.
- [28] Akhiezer, A. I., Akhiezer, I. A., Polovin, R. V., Sitenko, A. G., and Stepanov, K. N. 1975, *Plasma electrodynamics*, Vol. 1, Pergamon Press, Oxford.
- [29] Gogosov, V. V. 1961, Resolution of an arbitrary discontinuity in magnetohydrodynamics, *J. appl. math. Mech.*, 25, 148.
- [30] Petschek, H. E. 1964, Magnetic field annihilation, in *Physics of solar flares*, Hess, W. N. (ed.), NASA SP 50, 425.
- [31] Vasyliunas, V. M. 1975, Theoretical models of magnetic field line merging, 1, *Rev. Geophys. Space Sci.*, 13, 303.
- [32] Semenov, V. S., Kubyshekin, I. V., Rijnbeek, R. P., and Biernat, H. K. 2003, Analytical theory of unsteady Petschek-type reconnection, *Recent Res. Devel. Plasmas*, in press.
- [33] Penz, T. 2002, Remote sensing of flux transfer events based on the theory of ill-posed inverse problems, Diploma thesis, University of Graz, Austria.
- [34] Vladimirov, V. S. 1984, *Equations of mathematical physics*, Mir Publishers, Moscow.
- [35] Bronstein, I. N., and Semendjajew, K. A. 1996, *Teubner-Taschenbuch der Mathematik*, B. G. Teubner, Leipzig.
- [36] Tikhonov, A. N., and Goncharsky, A. V. (eds.) 1987, *Ill-posed problems in the natural sciences*, Mir Publishers, Moscow.
- [37] Hadamard, J. 1932, *Le problème de Cauchy et les équations aux dérivées partielles Linéaires Hyperboliques*, Hermann, Paris.
- [38] Semenov, V. S., Heyn, M. F., and Ivanov, I. B. 2003, Magnetic reconnection with space and time varying reconnection rates in a compressible plasma, *Phys. Plasmas*, in press.